Preliminary experimental study on a GW-level C-band relativistic magnetron

Haodong Xu(徐浩东), Kunpeng Chen(陈琨鹏), Zeyang Liu(刘则阳), Difu Shi(史迪夫), Yuwei Fan(樊玉伟)
Citation: Chin. Phys. B. 35, 108402 (2026). DOI: 10.1088/1674-1056/ae24ec | CSTR: 32038.14.CPB.ae24ec
http://cpb.iphy.ac.cn; http://iopscience.iop.org/cpb

What follows is a list of articles you may be interested in

A kinetic criterion for Stokes–Einstein relation breakdown based on effective collision al geometry

Zhen-Wei Wu(武振伟)
Chin. Phys. B. 35, 056402 (2026). DOI: 10.1088/1674-1056/ae32ff | CSTR: 32038.14.CPB.ae32ff

Designing a P2-type cathode material with Li in both Na and transition metal layers fo r Na-ion batteries

Jianxiang Gao(高健翔), Kai Sun(孙凯), Hao Guo(郭浩), Zhengyao Li(李正耀), Jianlin Wang(王建林), Xiaobai Ma(马小柏), Xuedong Bai(白雪东), Dongfeng Chen(陈东风)
Chin. Phys. B. 31, 098201 (2022). DOI: 10.1088/1674-1056/ac6b21

An improved secondary electrons energy spectrum model and its application in multipactor discharge

Wan-Zhao Cui(崔万照), Heng Zhang(张恒), Yun Li(李韵), Yun He(何鋆), Qi Wang(王琪), Hong-Tai Zhang(张洪太), Hong-Guang Wang(王洪广), Jing Yang(杨晶)
Chin. Phys. B. 27, 038401 (2018). DOI: 10.1088/1674-1056/27/3/038401

A low-outgassing-rate carbon fiber array cathode

An-Kun Li(李安昆), Yu-Wei Fan(樊玉伟), Bao-Liang Qian(钱宝良), Zi-Cheng Zhang(张自成), Tao Xun(荀涛)
Chin. Phys. B. 27, 028401 (2018). DOI: 10.1088/1674-1056/27/2/028401

Preliminary experimental study on a GW-level C-band relativistic magnetron

Haodong Xu(徐浩东), Kunpeng Chen(陈琨鹏), Zeyang Liu(刘则阳), Difu Shi(史迪夫), and Yuwei Fan(樊玉伟)†

College of Advanced Interdisciplinary Studies, National University of Defense Technology, Changsha 410073, *China*

(Received 6 September 2025; revised manuscript received 18 November 2025; accepted manuscript online 27 November 2025)

A C-band relativistic magnetron with an improved structure is investigated experimentally in this paper, which was proposed in the previous work. This magnetron adopts a periodically symmetric extraction structure, achieving strong coupling with non-π modes. It enables the single operation of the π mode, enhancing the stability and efficiency of the magnetron's operation. In the simulations, the microwaves are generated with a peak power of 2.53 GW and a power efficiency of 58.3%. In the initial experiments, the deposition of axial leakage current on the output inner conductor severely affected the operation of the CRMIS. By improving the structure of the output inner conductor, the effect of axial leakage current was mitigated. At a voltage of 537 kV and a magnetic field of 0.275 T, a diode current of 9.1 kA was obtained, and the microwave power reached 1.27 GW at a frequency of 4.367 GHz, corresponding to a power efficiency of 26%. However, when the diode voltage increased to 600 kV, a breakdown occurred between the anode vanes and the cathode cap.

Keywords: relativistic magnetron, breakdown, cathode caps

PACS: 84.40.Fe

DOI: 10.1088/1674-1056/ae24ec **CSTR:** 32038.14.CPB.ae24ec

1. Introduction

A relativistic magnetron (RM) with an all-cavity extraction structure has a compact structure.[1–4] Compared to the magnetron with diffraction output,[5–8] its extraction structure moves forward to the middle position of the resonant cavity, making the axial length of the RM shorter.[4] And its output mode is the TE_{11} mode in the sectorial waveguide, which can be converted conveniently to a TE_{11} conventional circular waveguide mode.[9]

In our laboratory, an L-band high-efficiency relativistic magnetron (HERM) with a novel all-cavity extraction structure was presented in 2019. In simulation, the power efficiency is 75.7%.[10] In the experiments, it can radiate microwave power of 1.3 GW with a power conversion efficiency of 40% at 1.47 GHz.[11] To expand RM's operation frequency, a C-band RM with an improved structure (CRMIS) was presented in previous work.[12] High-power microwaves are generated with a peak power of 2.53 GW, a frequency of 4.33 GHz, and a power efficiency of 58.3% when the voltage is 650 kV and the axial magnetic field is 0.347 T.

In this paper, the magnetron is investigated experimentally, driven by a 40 Ω, 50 ns pulse width accelerator, TORCH-01. In the initial experiments, the deposition of axial leakage current on the output inner conductor (shown in Fig. 1(a)) seriously affects the operation of the RM. By improving the structure of the output inner conductor, the effect of axial leakage current is reduced. When the voltage is 537 kV and the magnetic field is 0.275 T, the diode current is 9.1 kA and the microwave power is 1.27 GW at a frequency of 4.367 GHz, with a corresponding power efficiency of 26%. When the diode voltage increases to 600 kV, a breakdown occurs between the anode vanes and the cathode cap.

2. Model and simulations

The model of the C-band relativistic magnetron is illustrated in Fig. 1, and the dimensions are shown in Reference.[12] The C-band relativistic magnetron consists of ten anode vanes, a cathode with two endcaps, five microwave extraction slots, and a coaxial output waveguide. Note that the C-band relativistic magnetron adopts two kinds of anode vanes of different lengths to an improved extraction slot. Two kinds of anode vanes are arranged alternately. The long anode vanes connect with the inner conductor of the coaxial output waveguide, while the short ones do not.

The π mode is chosen to be the operating mode because of its non-degeneracy. The spatial symmetry of the output coupler facilitates the excitation of a pure π mode.[13] This connection structure short-circuits all long anode-vanes, like the strapped RM, which can increase the π-mode separation.[14] The fundamental modes of a magnetron (with N resonant cavities) are all TE waves, which can be defined as $H(n)$ modes, where n is the mode number and $n = 0, 1, 2, \ldots, N-1$. For the π mode, $n = N/2$. This periodic structure with $N/2$ periods, as shown in Fig. 1(d), breaks the independence of the

†Corresponding author. E-mail: fyw9108212@126.com

© 2026 Chinese Physical Society and IOP Publishing Ltd. All rights, including for text and data mining, AI training, and similar technologies, are reserved.

eigenmodes supported by the original N-fold symmetry, and the periodic boundary conditions force the reflected waves to satisfy specific phase matching. Therefore, when the $H(n)$ mode is incident on this structure, it will reflect another mode $H(|N/2-n|)$ in addition to itself, interfering with the normal operation of the $H(n)$ mode.[14] However, the π mode is not affected by such interference, because the electric field of the π mode satisfies both N-fold symmetry and $N/2$-fold symmetry. This enables the π mode to operate stably once established, while non-π modes are disturbed by the reflected modes.

Even if the π-mode separation is 1%, the π mode can also be excited independently.[13–15] In simulations, the C-band relativistic magnetron's operating frequencies of the π mode and the $(\pi-1)$ mode are 4.33 GHz and 3.98 GHz, respectively, and the corresponding π-mode separation is 8%. Accordingly, as for the C-band relativistic magnetron with the traditional full-cavity extraction structure, the operating frequencies of the π mode and the $(\pi-1)$ mode are 4.35 GHz and 4.10 GHz, respectively, and the corresponding π-mode separation is 5%. Hence, this design is advantageous for suppressing mode competition.

Figures 1(c) and 1(d) provide the cross sections of the interaction region and the extraction slots, respectively. Microwaves are generated in the interaction region and radially coupled from the extraction slot into the sectorial waveguide. In the sectorial waveguide (Fig. 1(e)), the wave function of the TE modes is given by[16]

$$V(\rho,\varphi,z) = V_0\left[N'_\nu(Tr_\mathrm{o})J_\nu(T\rho)-J'_\nu(Tr_\mathrm{o})N_\nu(T\rho)\right]\cos\nu\varphi\cdot \mathrm{e}^{-\mathrm{j}\beta z}, \quad (1)$$

where r_o, r_i, and θ_s are shown in Fig. 1. T, ν, and β are determined by the following equations:

$$\nu = \frac{n\pi}{\theta_\mathrm{s}}, \quad n=0,1,2,3\ldots, \quad (2)$$

$$J'_\nu(Tr_\mathrm{i})N'_\nu(Tr_\mathrm{o})-J'_\nu(Tr_\mathrm{o})N'_\nu(Tr_\mathrm{i})=0, \quad (3)$$

$$\beta=\omega^2\mu\varepsilon-T^2. \quad (4)$$

Here, ω, μ, and ε are the angular frequency, permeability, and dielectric constant, respectively. Equation (3) is the eigen equation of TE_{nm} modes, and T is the m-th root of (3). Therefore, when the width of the sectorial waveguide is constant, the TE_{11} mode will be excited, and the other modes will be suppressed by adjusting the inner radius and outer radius of the sectorial waveguide.[17]

In the coaxial waveguide, the TE_{11} mode in the sectorial waveguide is easy to convert to the TEM mode because of the same phase and amplitude in multiple sector waveguides of the all-cavity extracted structure. In the experiments, the TEM mode will be converted to the TM_{01} by a mode converter and radiated by a conical horn antenna.

The typical simulation results are shown in Fig. 2. With a magnetic field of 0.347 T, an applied voltage of 650 kV, and a current of 6.1 kA, the input power was 4.34 GW. The peak output power reached 2.53 GW, corresponding to a power efficiency of 58.3%. The operating mode was the π mode, and the microwave frequency was 4.35 GHz.

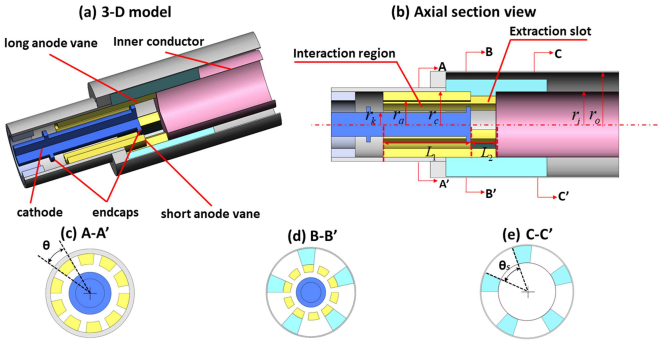

Fig. 1. The model of C-band relativistic magnetron. (a) The 3-D model. (b) Axial section view of C-band relativistic magnetron; (c) cross section view of A–A′; (d) cross section view of B–B′; (e) cross section view of C–C′.

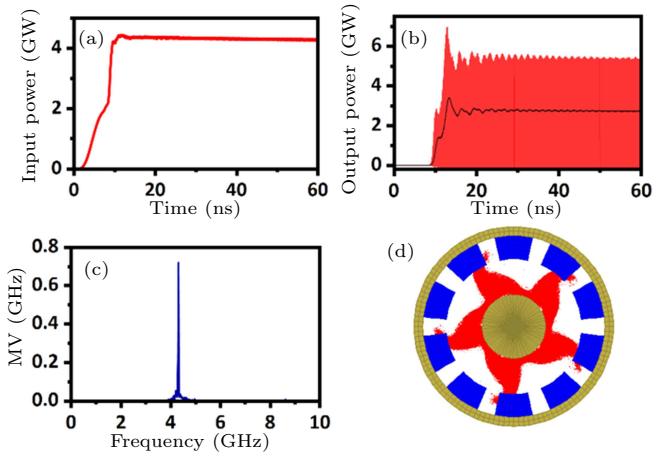

Fig. 2. The typical simulation results. (a) Input power; (b) output power; (c) spectrum of C-band relativistic magnetron; (d) electronic spoke of the π mode.

3. Preliminary experiments results

The experimental setup and equipment, depicted in Fig. 3(a), mainly consist of a pulsed power source, an HPM source (C-band relativistic magnetron), a magnet system, a radiating antenna, and a microwave measurement system. In addition, the background pressure must be less than 5×10^{-3} Pa. The C-band relativistic magnetron was fabricated according to the structure designed in the simulation works. Figure 3(b) presents a photograph of the C-band relativistic magnetron and its key components.

The accelerator, TORCH-01, is composed of a Tesla transformer and a transmission line, which can provide a pulse range from 300 kV to 600 kV with a duration of 50 ns, several GW of pulsed power, and the impedance of the transmission line is about 40 Ω. The axial magnetic field is provided by a solenoid magnet that has a 100-mm axial uniform area.

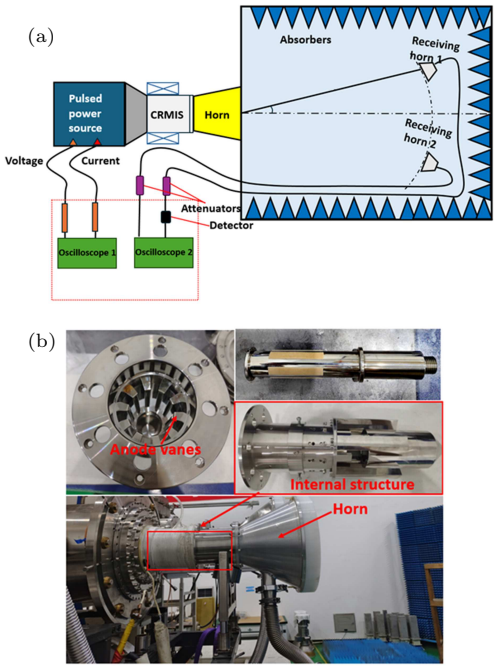

Fig. 3. (a) The experimental layout. (b) Picture of CRM and some key components.

The horn antenna was designed according to the output mode and the operating frequency of the C-band relativistic magnetron. The antenna output aperture D is 340 mm, and the length is 230 mm. Its output mode is TM_{01}, and the main lobe is at 7° with a gain G of 17.1 dB. As for the receiving antenna, it should be placed in the far-field position away from the radiating horn antenna. The far-field distance R depends on the horn aperture D and the wavelength of the radiated microwave λ, which is

$$R \geq \frac{2D^2}{\lambda}. \tag{5}$$

So, R should be longer than 3.55 m, when $D = 340$ mm and $\lambda = 69$ mm. And in the experiment, the R is 5 m. Assuming that the C-band relativistic magnetron operates stably in the π mode and the output mode of the horn antenna is TM_{01} mode, the microwave power. By measuring the power density received at this horn (at the main lobe), the microwave power P_o is obtained as

$$P_o = \frac{4\pi R^2 P_i 10^{(G_a/10)}}{A_e 10^{(G/10)}}, \tag{6}$$

where P_i is the power value received at the detector, A_e is the effective area of the receiving horn, G is the gain of the transmitting horn at the main lobe angle, and G_a is the total attenuation between the receiving horn and the detector shown in Fig. 3(a).

In the initial experiments, the deposition of axial leakage current on the output inner conductor had a significant impact on the C-band relativistic magnetron operation. The unexpected electron emission ensuing from the breakdown will significantly affect the working performance of the C-band relativistic magnetron.[17–22] The simulation results and the experimental results are shown in Fig. 4(a). Because of the axial leakage current, the traces of electron flow bombardment on the surface of the inner conductor were clearly visible after dozens of shots when the voltage was about 450 kV. The experimental results demonstrate that anode plasma was generated. The ion flow from the inner conductor plasma (anode plasma) bombards the cathode cap, leading to cathode cap damage, which can cause shortened microwave pulses.[21]

For the inner conductor made of stainless steel, the dose of the electron energy deposition on the surface (ρ'_E) is one of the key factors for measuring whether the anode suffers breakdown damage.[23,24] For common metals, the threshold of ρ'_E is generally in the range of 100 J/g,[25] and the ρ'_E can be obtained from the following formula:

$$\rho'_E = \frac{\rho_E}{\rho R}, \tag{7}$$

where ρ_E is the energy density (J/cm^2):

$$\rho_E = \frac{U I_a \tau}{S}, \tag{8}$$

where U and I_a are the voltage and the axial leakage current, and τ is the duration of the average axial current, which is about 50 ns. S is the area of the region that is bombarded. It can be seen from Fig. 4(a) that the shape of the bombarded region is an annulus. Its approximate area is 1.53 cm^2.

And ρR is the continuous slowing-down approximation for electrons, which is given by[26]

$$\rho R = 0.526E - 0.094 = 0.1164\ (\mathrm{g/cm^2}), \tag{9}$$

where ρ is the density of the metal and R is the range of the electron, and $E = 0.4$ MeV (the operating voltage here is set at 400 kV) is the initial energy of the electrons.

Therefore, the axial current damage threshold can be expressed as

$$I_a = \frac{\rho_E S}{\tau U} \approx 890\ (\mathrm{A}). \tag{10}$$

For the axial current of a relativistic magnetron, it is easy to exceed the threshold of 0.89 kA, resulting in anode plasma generation. To prevent such a situation from occurring, the options are to increase the receiving area (S) or to increase the damage energy threshold by changing the material.

To address this issue, a hole was drilled in the inner conductor. Figure 4(b) shows the simulation result (left) and the modified physical object (right). The leakage currents are axially transported to regions with a smaller magnetic field, resulting in a more dispersed current and a larger current-receiving area, thereby preventing plasma generation. Moreover, the change in the inner conductor did not affect the operating state in simulations, and in the experiments, the C-band relativistic magnetron operation became stable with the new inner conductor.

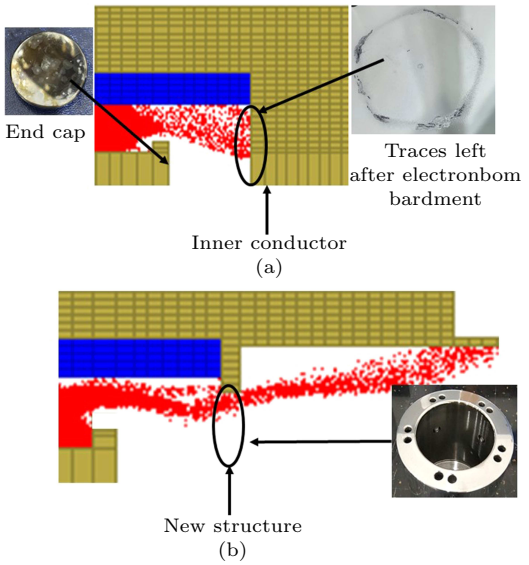

Fig. 4. The improvement of the inner conductor. (a) The breakdown between the cap and the inner conductor and simulation. (b) The new structure of the inner conductor.

Figures 5(a)–5(d) present the experimental results of the C-band relativistic magnetron. At a voltage of 537 kV and a magnetic field of 0.275 T, the diode current was 9.1 kA (Fig. 5(a)). The amplitudes of the two detected signals were 131 mV and 129 mV. Using Eq. (6), the measured powers were 1.29 GW and 1.25 GW, respectively, with a corresponding power efficiency of 26% (Fig. 5(b)). More intuitively, Fig. 5(c) shows the microwave signal not detected by the detector, and Fig. 5(d) shows its spectrum. The microwave pulse width was approximately 28 ns, and the corresponding frequency was 4.367 GHz.

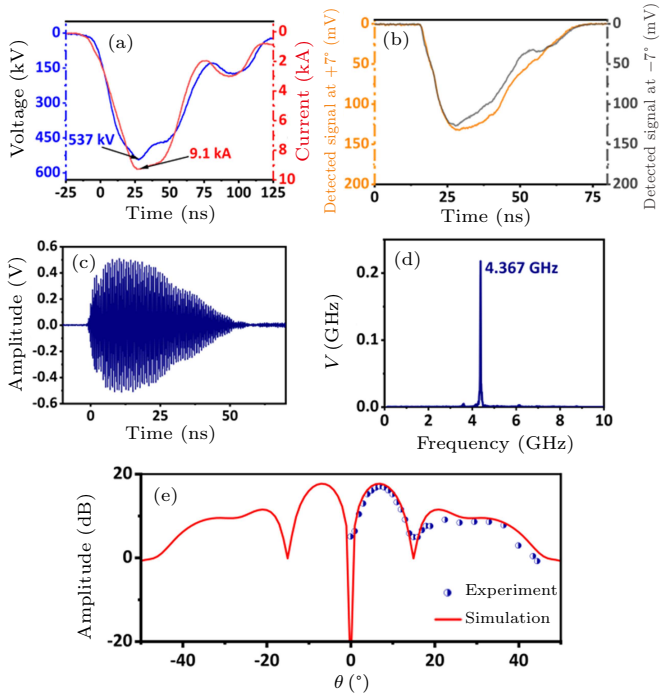

Fig. 5. The experimental results of CRM. (a) Voltage and current; (b) two detected microwave channels at the main lobe (±7°); (c) the microwave signal; (d) spectrum; (e) radiation pattern.

The radiation pattern can help us judge whether the C-band relativistic magnetron works in the π mode and the purity of the radiation mode. The measurement method is to fix a receiving horn at the maximum radiation direction angle of 7°, and the stability of the output performance of the C-band relativistic magnetron is confirmed by monitoring the microwave signal received at this horn. The other receiving horns were placed every 1 degree from 0° to 21°, and every 3.5 degrees from 21° to 45.5°. Figure 5(e) compares the measurement and simulation results. The experimental pattern was nearly consistent with the simulated pattern, indicating that the CRMIS output mode was a pure TEM mode.

However, when the voltage increased to around 600 kV, there was a breakdown between the cathode cap and the anode, so the microwave power was not further improved, as shown in Fig. 6(a). This was because the 10-mm gap between the cathode cap and the anode was too narrow. To suppress the radial breakdown of the cathode and anode, an attempt was made to shorten the radius of the cathode cap by 2 mm. This will greatly reduce the risk of breakdown. Meanwhile, the cathode caps and anode vanes were reprocessed, with larger chamfers added at the edges prone to breakdown, as shown in Figs. 6(b) and 6(c). The new cathode cap and anode vanes feature larger chamfer radii at their radial edges, further reducing the breakdown risk.

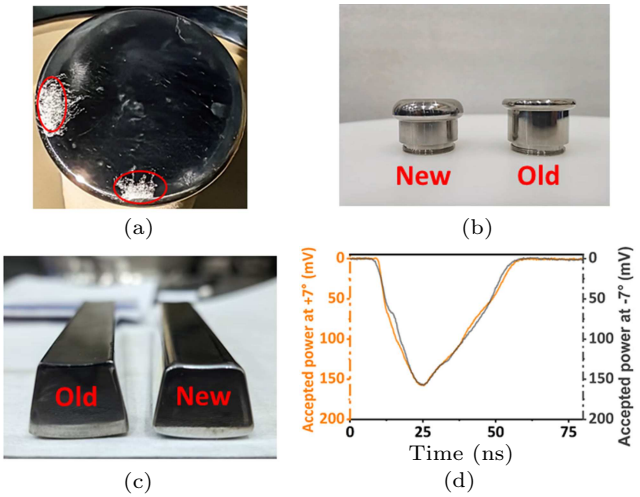

Fig. 6. Breakdown phenomenon and improved experimental results. (a) Breakdown marks on the cathode cap; (b) the caps; (c) the anode vanes; (d) two detected microwave channels at the main lobe (±7°).

When the voltage is increased to 605 kV with a matched magnetic field of 0.305 T, the diode current reaches 10.8 kA accordingly. Experimental results show that the aforementioned improvement measures have alleviated the previous breakdown issue, enabling the RM to operate stably. Figure 6(d) presents the microwave detected signal at this voltage, with two power amplitudes of 158 mV and 157.5 mV, corresponding to powers of 1.44 GW and 1.43 GW, respectively. However, a comparison between Figs. 5(b) and 6(d) reveals a significant reduction in the pulse width of the latter, along

with a drop in power efficiency to 22%. The reduced radius of the cathode cap weakens the cathode's ability to constrain electrons, leading to a decrease in efficiency. Regarding the pulse shortening, we believe that although no obvious breakdown phenomenon was observed in the experimental results of Fig. 6, unintended radial electron emission still occurred in practice. It can be clearly observed that the impedance at 605 kV (56 Ω) is lower than that at 537 kV (60 Ω), indicating that the current is slightly higher than expected. Although increasing the magnetic field can raise the impedance, the voltage and magnetic field will no longer be matched, resulting in a decrease in output power.

4. Conclusion and perspectives

In conclusion, this paper experimentally demonstrated the C-band relativistic magnetron. Initial breakdown issues were resolved by improving the output inner conductor structure, resulting in stable C-band relativistic magnetron operation. The C-band relativistic magnetron achieved a microwave output of 1.27 GW with a power efficiency of 26%. However, a breakdown occurred between the anode vanes and the cathode cap when the diode voltage reached 600 kV.

To suppress the breakdown observed in the experiments, the gap between the anode and cathode can be increased or the tip emission factor can be reduced, such as by chamfering the anode vanes and the cathode cap. We adopted this method in subsequent experiments, which indeed increased the power threshold of the RM. At 605 kV, the output power reached 1.44 GW, but the efficiency did not improve further. Meanwhile, through calculations of current and impedance, we found that unintended current emission still occurred. Alternatively, modifying the cathode material (e.g., adopting a carbon fiber cathode) and applying specialized coatings on the surfaces of both the anode and cathode can significantly increase the breakdown threshold.[27]

References

[1] Benford J, Swegle J and Schamiloglu E 2015 *High Power Microwaves* 3rd edn(New York: Taylor & Francis) pp. 231–274

[2] Schamiloglu E 2004 *Proc. 2004 IEEE MTT-S Int. Microwave Symp.*Vol. 2 (IEEE) pp. 1001–1004

[3] Andreev D, Kuskov A and Schamiloglu E 2019 *Matter and Radiation at Extremes* **4** 067201

[4] Hoff B W, Greenwood A D, Mardahl P J and Haworth M D 2012 *IEEE Trans. Plasma Sci.* **40** 3046

[5] Kovalev N, Kol'chugin B, Nechaev V, Ofitserov M, Soluyanov E and Fuks M 1977 *Sov. Tech. Phys. Lett.* **3** 430

[6] Fuks M I and Schamiloglu E 2010 *IEEE Trans. Plasma Sci.* **38** 1302

[7] Zhao L, Qian B L, Li R and Du G X 2008 *Chin. Phys. C* **32** 268

[8] Leach C, Prasad S, Fuks M I, Buchenauer C J, McConaha J and Schamiloglu E 2017 *IEEE Trans. Plasma Sci.* **45** 282

[9] Yang W, Dong Y and Dong Z 2016 *Acta Phys. Sin.* **65** 248401 (in Chinese)

[10] Liu Z, Fan Y, Wang X, Shi D, Li A and Yu Y 2020 *AIP Adv.* **10** 035104

[11] Liu Z, Fan Y, Xu H, Li A, Wang X and Shi D 2022 *Rev. Sci. Instrum.* **93** 104710

[12] Xu H, Wang X, Liu Z, Li A and Fan Y 2023 *IEEE Trans. Electron Devices* **70** 1270

[13] Boot H A H 1961 in *Crossed Field Microwave Devices* Okress E 2nd edn (New York: Academic Press) pp. 261–274

[14] Pickering A H 1961 in *Crossed Field Microwave Devices* Okress E 2nd edn (New York: Academic Press) pp. 275–290

[15] Prasad S, Galbreath D, Fuks M and Schamiloglu E 2010 *Proc. 2010 IEEE Int. Vacuum Electron. Conf.* (Monterey, CA) pp. 379–380

[16] Zhang K and Li D 2008 in *Electromagnetic Theory for Microwaves and Optoelectronics*(Beijing: Publishing House of Electronics Industry) pp. 255–259

[17] Liu Q and Yuan C 2005 *High Power Laser Part. Beams* **17** 897

[18] Yu B, Liang W, Jiao J, Kang X L and Zhao Q 2019 *Acta Phys. Sin.* **68** 070201 (in Chinese)

[19] Fuks M I, Andreev D A, Kuskov A and Schamiloglu E 2019 *Plasma* **2** 222

[20] Hegeler F, Friedman M, Myers M C, Sethian J D and Swanekamp S B 2002 *Phys. Plasmas* **9** 4309

[21] Hegeler F, Friedman M, Myers M C, Swanekamp S B and Sethian J D 2001 *Proc. 28th IEEE Int. Conf. Plasma Sci.* (IEEE)

[22] Miller R B 1998 *J. Appl. Phys.* **84** 3880

[23] Fan Y, Zhong H, Yang H, Li Z, Shu T, Zhang J, Wang Y and Luo L 2008 *J. Appl. Phys.* **103** 123301

[24] Sanford T W L, Halbleib J A, Poukey J W, Pregenzer A L, Pate R C, Heath C E, Mock R, Mastin G A, Ghiglia D C, Roemer T J, Spence P W and Proulx G A 1989 *J. Appl. Phys.* **66** 10

[25] Cuneo M E, Menge P R and Hanson D L 1997 *IEEE Trans. Plasma Sci.* **25** 229

[26] Shultis J K and Faw R E 2002 *Fundamentals of Nuclear Science and Engineering* (New York: Dekker) pp. 132–135

[27] Chandra R, Roy A, Kalyanasundaram S, Patel A S, Sharma V K, Menon R, Pasula N, Kumar R, Ventizenko I and Mashchenko A 2014 *IEEE Trans. Plasma Sci.* **42** 3491